© The American Society of Gene & Cell Therapy

PET Imaging of Oncolytic VSV Expressing the Mutant HSV-1 Thymidine Kinase Transgene in a Preclinical HCC Rat Model

Kim A Muñoz-Álvarez[1], Jennifer Altomonte[1], Iina Laitinen[2], Sibylle Ziegler[2], Katja Steiger[3], Irene Esposito[3], Roland M Schmid[1] and Oliver Ebert[1]

[1]II. Medizinische Klinik und Poliklinik, Klinikum rechts der Isar, Technische Universität München, München, Germany; [2]Nuklearmedizinische Klinik und Poliklinik, Technische Universität München, München, Germany; [3]Institut für Allgemeine Pathologie und Pathologische Anatomie, Technische Universität München, München, Germany

Hepatocellular carcinoma (HCC) is the most predominant form of liver cancer and the third leading cause of cancer-related death worldwide. Due to the relative ineffectiveness of conventional HCC therapies, oncolytic viruses have emerged as novel alternative treatment agents. Our previous studies have demonstrated significant prolongation of survival in advanced HCC in rats after oncolytic vesicular stomatitis virus (VSV) treatment. In this study, we aimed to establish a reporter system to reliably and sensitively image VSV in a clinically relevant model of HCC for clinical translation. To this end, an orthotopic, unifocal HCC model in immune-competent Buffalo rats was employed to test a recombinant VSV vector encoding for an enhanced version of the herpes simplex virus 1 (HSV-1) thymidine kinase (sr39tk) reporter, which would allow the indirect detection of VSV via positron emission tomography (PET). The resulting data revealed specific tracer uptake in VSV-HSV1-sr39tk–treated tumors. Further characterization of the VSV-HSV1-sr39tk vector demonstrated its optimal detection time-point after application and its detection limit via PET. In conclusion, oncolytic VSV expressing the HSV1-sr39tk reporter gene allows for highly sensitive *in vivo* imaging via PET. Therefore, this imaging system may be directly translatable and beneficial in further clinical applications.

Received 8 August 2014; accepted 12 January 2015; advance online publication 17 February 2015. doi:10.1038/mt.2015.12

INTRODUCTION

Hepatocellular carcinoma (HCC) is a globally spread malignant disease with rising incidence in the United States and Europe.[1–3] Curative treatments are limited to liver resection, local ablation or liver transplantation, for which only a very small percentage of patients are candidates. Most patients present themselves with advanced disease at the time of detection and are only eligible for palliative treatments, which offer poor prognoses.[2–4] This situation ranks HCC the third leading cause of cancer-related death worldwide,[5,6] and novel treatment options are urgently needed.

Oncolytic virus (OV) therapy is a promising new strategy in cancer therapy. OVs are naturally occurring viruses named for their property to preferentially replicate in cancerous cells, while leaving healthy cells mainly unaffected.[7] With increasing momentum over the last 15 years, OVs have been in the focus of cancer research, and their overall success has been well documented[8,9] and has culminated in a wave of clinical trials of many different vector platforms for various cancers, including HCC.[10–13] One such promising OV is vesicular stomatitis virus (VSV).[14] Our previous studies have demonstrated significant prolongation of survival in HCC-bearing rats after VSV treatment.[15–17] More recently, we have reported that VSV treatment of HCC in the clinically relevant context of hepatic fibrosis, is not only safe, but it also provides a therapeutic benefit to the underlying liver pathology.[18] Additionally, a phase 1 clinical trial, using recombinant VSV expressing interferon-β,[19] has recently been initiated in primary liver cancer patients (ClinicalTrials.gov Identifier: NCT01628640). As VSV virotherapy for HCC is becoming a reality, the necessity of a system to enable noninvasive and real-time monitoring of virus replication and biodistribution in patients has become apparent.

Noninvasive imaging is a technology, which allows us to monitor processes occurring inside the body without applying invasive procedures such as biopsies. Hybrid imaging of PET (positron emission tomography) and CT (computed tomography) is a modality routinely applied in the clinic, where the CT provides anatomical background information, while biological processes are detected by PET. PET enables the quantitative detection of radiotracers on a molecular level and, therefore, is suitable for monitoring biological processes via artificially introduced reporters,[20] such as the herpes simplex virus 1 (HSV1) thymidine kinase (TK). Vectors equipped with HSV1-TK are detectable by PET after application of an appropriate radionuclide-labeled tracer. Various radiotracers are available for the detection of the TK reporter by PET.[21,22] Although wild-type (wt) TK has been used for the detection of intrahepatic targets before in combination with other tracers,[23,24] we decided to exploit a mutant version of this reporter, sr39tk, which has been shown to have enhanced

Correspondence: Oliver Ebert, II. Medizinische Klinik und Poliklinik, Klinikum rechts der Isar, Technische Universität München, Ismaninger Str. 22, 81675 München, Germany. E-mail: oliver.ebert@lrz.tum.de

© The American Society of Gene & Cell Therapy

affinity and phosphorylation properties in comparison to the wt version.[25] Since we were seeking to establish a clinically translatable tool, we decided to employ an ^{18}F-labeled tracer with appropriate half-life (*i.e.*, 109.8 minutes) for clinical application, such as ^{18}F-FHBG (9-(4-[18F]-fluoro-3-[hydroxymethyl] butyl)guanine). The combination of the HSV1-sr39tk reporter with ^{18}F-FHBG has been successfully applied in imaging studies with hepatic targets, which can present unique challenges due to high background signals.[26,27] Importantly, ^{18}F-FHBG has been defined as one of the most favorable tracers for detection of the TK reporter, showing superior selectivity in comparison to other tracers.[28,29] Additionally, its safety was defined preclinically, and favorable pharmacokinetics and dosimetry have been demonstrated in humans.[30,31]

For this reason, we have engineered a recombinant VSV vector encoding the HSV1-sr39tk reporter (rVSV-HSV1-sr39tk) and tested its potential for noninvasive imaging of the virus in a clinically relevant model of orthotopic HCC in immune-competent rats.

Since the efficacy of various recombinant oncolytic VSV vectors in this HCC model has already been extensively demonstrated by our group,[15–17] this study concentrates exclusively on the establishment of the noninvasive *in vivo* imaging of the newly established reporter virus. Our results demonstrate that this system is highly sensitive, with minimal background in the liver setting, and allows for accurate monitoring of virus replication and distribution via ^{18}F-FHBG-PET and CT. These data support the application of the HSV1-sr39tk reporter for imaging of oncolytic VSV therapy in HCC patients in the future.

RESULTS

In vitro characterization of VSV-HSV1-sr39tk and HSV1-sr39tk–expressing stable rat HCC cell line

After successful cloning and rescue of rVSV-HSV1-sr39tk, the replication kinetics were assessed by *in vitro* multicycle and one-step growth curves (MOI: 0.01 and 10, respectively), using the previously established rVSV-lacZ as a control. The viral titers of both vectors were indistinguishable at all times points tested, indicating that the expression of the HSV1-sr39tk reporter gene does not alter viral kinetics (**Figure 1a**). Additionally, cell survival of rat HCC cells revealed no appreciable difference in the cytotoxicity of rVSV-HSV1-sr39tk as compared to the control vector (**Figure 1b**).

For the establishment of PET/CT imaging via the HSV1-tk reporter, an HCC cell line, stably expressing the reporter was generated to serve as a positive control. To confirm HSV-1-sr39tk protein expression in virus-infected and stably transfected cells, immunofluorescence microscopy (**Figure 1c**) and Western Blot analysis (**Figure 1d**) were performed. Both assays revealed protein expression specifically in the stable cell line and rVSV-HSV1-sr39tk–infected cells, while none could be detected in the control samples. Additionally, only the VSV-infected cells showed a positive VSV-G-protein signal.

To test the functionality of the expressed reporter protein, *in vitro* uptake of ^{18}F-FHBG was performed. Although untreated wt cells and cells infected with VSV-lacZ showed a very low background FHBG uptake, significantly higher tracer uptake could be detected in the stable cell line, as well as in the rVSV-HSV1-sr39tk–infected cells (**Figure 1e**).

Stable HSV1-tk–expressing subcutaneous tumors result in significant uptake of ^{18}F-FHBG

To establish the PET/CT imaging protocol, animals were implanted with two subcutaneous tumors: a stable HSV1-tk–expressing HCC cell line on the right and the wt HCC cell line on the left shoulder (N = 4). FHBG-PET/CT imaging revealed strong signals in tumors of the stable cell line, while there was no observable signal in wt tumors (**Figure 2a**). Quantitative ROI analysis demonstrated a significant FHBG tracer uptake in the stable tk-expressing tumors (**Figure 2b**). These findings were confirmed by *ex vivo* immunohistochemistry and autoradiography. While wt tumors showed no HSV-tk expression by immunohistochemistry and autoradiography, stable tumors showed a positive signal by both methods (**Figure 2c**). Importantly, overlaying immunohistochemistry and autoradiography images revealed a colocalization of HSV1-tk expression with tracer uptake. Semiquantitative analysis by autoradiography additionally illustrated a significant tracer uptake only in the stable tumors (**Figure 2d**).

Intratumoral injection of rVSV-HSV1-sr39tk results in significant ^{18}F-FHBG-PET signals in orthotopic HCC

To determine the applicability of rVSV-HSV1-sr39tk imaging to the orthotopic system, intrahepatic HCC tumors were injected with PBS (N = 4), or 10^7 pfu of rVSV-lacZ (N = 2) or rVSV-HSV1-sr39tk (N = 6). As a positive control, a group of rats was implanted with stable HSV1-sr39tk–expressing HCC cells (N = 3). No signal was detected in PBS or VSV-lacZ–treated tumors via FHBG-PET/CT 1 day after treatment, while high tracer uptake could be seen in positive control animals, as well as in rVSV-HSV1-sr39tk–treated animals (**Figure 3a**). Semiquantitative ROI analysis of these data revealed significant FHBG tracer uptake in the stable tk-expressing tumors and rVSV-HSV1-sr39tk–treated tumors compared to liver, while control-treated tumors showed no increase (**Figure 3b**). To validate these findings, we performed *ex vivo* immunohistochemistry and autoradiography. Positive staining for HSV-tk could be observed only in tumors of the stable cell line or those treated with rVSV-HSV1-sr39tk, which correlated to areas of tracer uptake on corresponding autoradiography images (**Figure 3c**). Semiquantitative analysis of autoradiography data illustrated significant tracer uptakes in the stable tumors and rVSV-HSV1-sr39tk–treated tumors only (**Figure 3d**).

The tumor signal in ^{18}F-FHBG-PET peaks on day 1 after VSV-HSV1-sr39tk treatment

To investigate the kinetics of VSV-mediated HSV1-sr39tk imaging, HCC-bearing animals were injected intratumorally with 10^7 pfu VSV-HSV1-sr39tk and imaged either 6 hours (N = 2), 1 day (N = 4) or 3 days (N = 5) after virus treatment by FHBG-PET/CT (**Figure 4a**). While no specific tumor signal could be detected 6 hours after virus application, a strong intratumoral ^{18}F-FHBG uptake could be detected 1 day after therapy, which was statistically significant by ROI analysis (**Figure 4b**). Although tumor ROI values remained statistically significant on day 3, the intensity had decreased to a similar level to that observed after 6 hours,

© The American Society of Gene & Cell Therapy

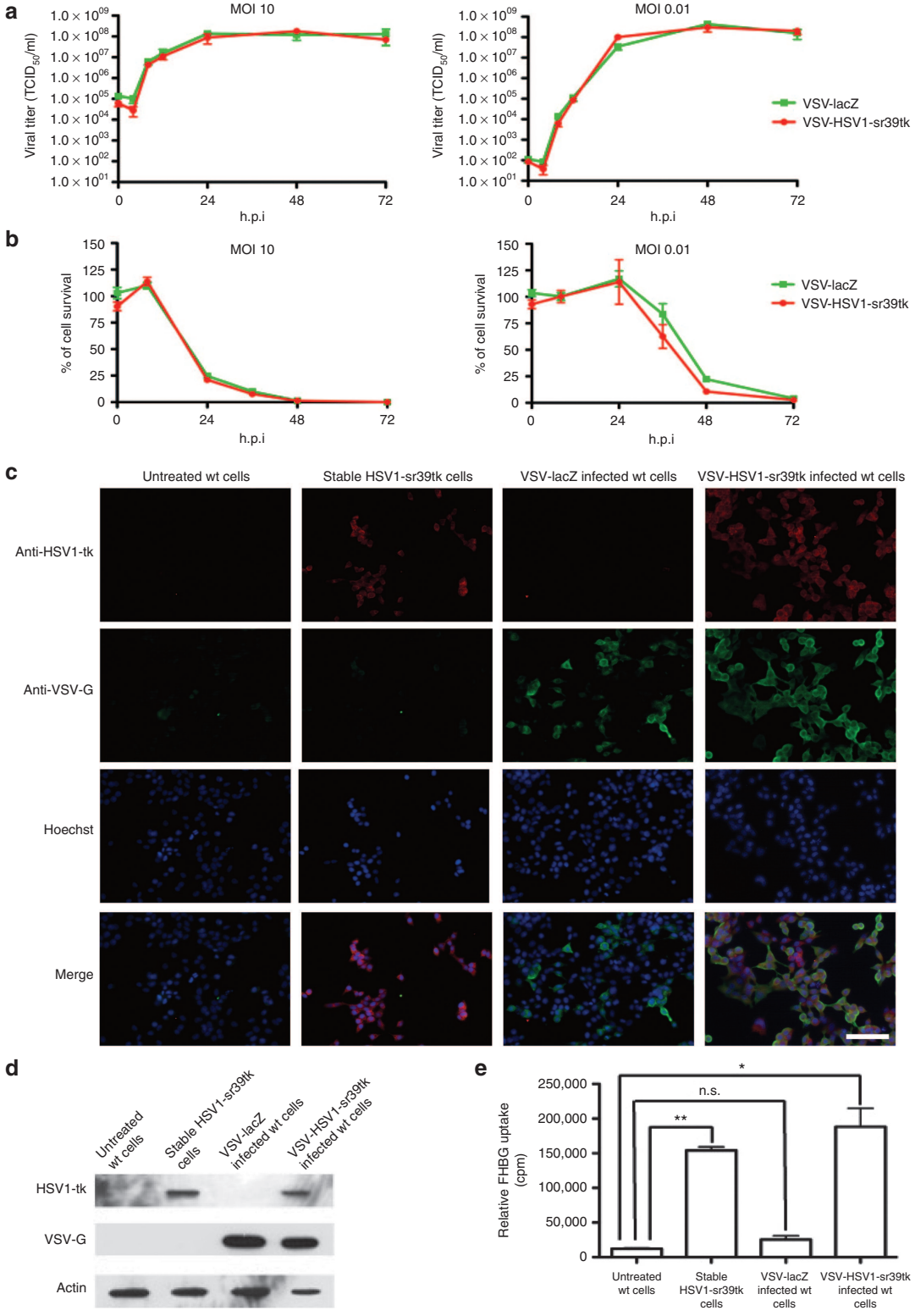

Figure 1 *In vitro* characterization of the HSV1-sr39tk reporter. (**a**) One-step (left panel) and multistep (right panel) growth curves of rVSV-lacZ (green) and rVSV-HSV1-sr39tk (red) in cultured rat HCC cells after an infection at either MOI 10 (one-step) or MOI 0.01 (multistep). Supernatants were collected at different hours postinfection (h.p.i.), and titer was determined by $TCID_{50}$ assay on BHK cells. (**b**) Cell survival assay of rat HCC cells after an infection at either MOI 10 (left panel) or MOI 0.01 (right panel) by MTS assay. (**c**) Indirect immunofluorescence of cultured cells and (**d**) Western Blot of whole cell lysates of untreated wt rat HCC cells, stably HSV1-sr39tk–expressing rat HCC cells and either VSV-lacZ or VSV-HSV1-sr39tk–infected rat HCC cells. Microscopy has been performed at a magnification of 20×, and scale bar refers to 100 µm. (**e**) *In vitro* ^{18}F-FHBG tracer uptake of same samples as mentioned for **c** and **d**. All quantitative data represents the mean of triplicate samples ± SEM. Stars indicate significance with *P* values lower than 0.0001 (**) and lower than 0.0005 (*).

© The American Society of Gene & Cell Therapy

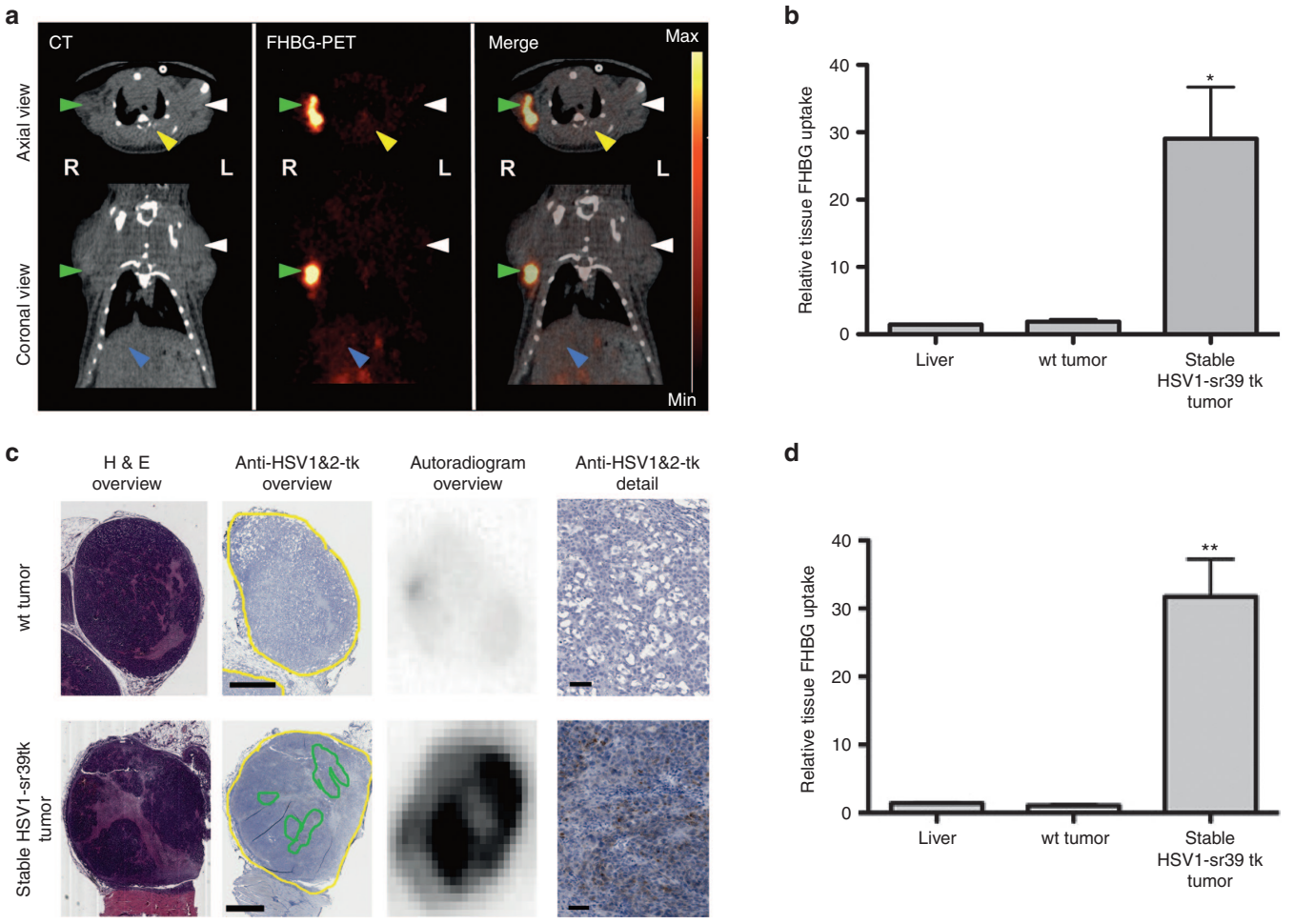

Figure 2 FHBG-PET/CT of subcutaneous HCC stably expressing the HSV1-sr39tk reporter. (**a**) Representative PET/CT image of a rat bearing subcutaneous tumors in both flanks in axial (upper panel) and coronal (lower panel) view. Signals of CT and PET are shown separately, as well as a merged image of both signals. Arrow heads indicate tumors (green: stable HSV1-sr39tk–expressing tumor on the right (R) side; white: wt tumor on the left (L) side), liver (blue) and spinal muscle (yellow). PET intensity scale is set to 3×10^5 Bq/ml at maximum value and 0 Bq/ml at minimum value. (**b**) Semiquantitative analysis of tracer accumulation in regions of interest (ROI) from PET/CT scans. (**c**) *Ex vivo* analysis of tumor sections (wt and stable tumor of the same animal). From left to right: HE-stained overview, anti-HSV-1&2-tk–stained overview (tumor encircled in yellow, areas of high HSV1&2-tk signal encircled in green) and autoradiogram of the same slice, followed by a detailed image of the anti-HSV-1&2-tk–stained tumor section. Scale bars: 1 mm (overview); 50 µm (detail). (**d**) Semiquantitative analysis of tracer accumulation in tissues of interest from *ex vivo* autoradiography analysis. All quantitative data is expressed as mean with SEM ($n = 4$) of the relative FHBG uptake in the indicated tissues, normalized to muscle. Stars indicate significance with P values lower than 0.01 (*) and 0.001 (**).

and no tumor signal could be detected visually. This data is consistent with our previous reports describing the replication kinetics of VSV in orthotopic HCC tumors, in which we observed a peak in viral titer on day 1, followed by a reduction by several logs on day 3.[17,32]

A viral dose of at least 1×10^6 pfu needs to be injected in order to guarantee successful detection of VSV-HSV1-sr39tk by PET

To determine the minimal injected viral load to receive a significant FHBG-PET signal, we performed a dose decrement study of VSV-HSV1-sr39tk. Starting at the maximum tolerated dose (MTD) of 10^7, orthotopic HCC-bearing rats were randomly assigned to receive log-wise dose decrements to a minimum dose of 10^4 pfu, with PBS as a control (PBS $N = 2$; 1×10^4 $N = 2$; 1×10^5 $N = 4$; 1×10^6 $N = 3$; 1×10^7 $N = 2$). On day 1 after treatment, significant tumor-to-liver signals were detected in the groups treated with a viral dose of 10^6 and 10^7, while lower doses resulted in no appreciable tracer uptake (**Figure 5a**). Similarly, quantitative ROI analysis revealed that the intratumoral tracer uptake was statistically significant with a minimum injection dose of 10^6 pfu (**Figure 5b**). Importantly, a goodness of fit analysis of PET tumor-to-liver ratios versus intratumoral viral titers revealed a strong correlation ($R^2 = 0.8880$) in animals treated with either 10^6 or 10^7 pfu of VSV-HSV1-sr39tk (**Figure 5c**).

In order to define a detection limit, the mean tumor-to-liver ratio of PBS-treated animals ($N = 6$) has been calculated. The mean value plus the standard deviation of this group resulted in y = 1.33 (**Figure 5d**). This is considered to be the background signal of untreated tumors, and we define any tumor-to-liver ratio greater than this value to be above the detection limit. To illustrate the signal distribution, intratumoral titers have been depicted against the respective tumor-to-liver-ratio in the individual animals (**Figure 5d**).

© The American Society of Gene & Cell Therapy

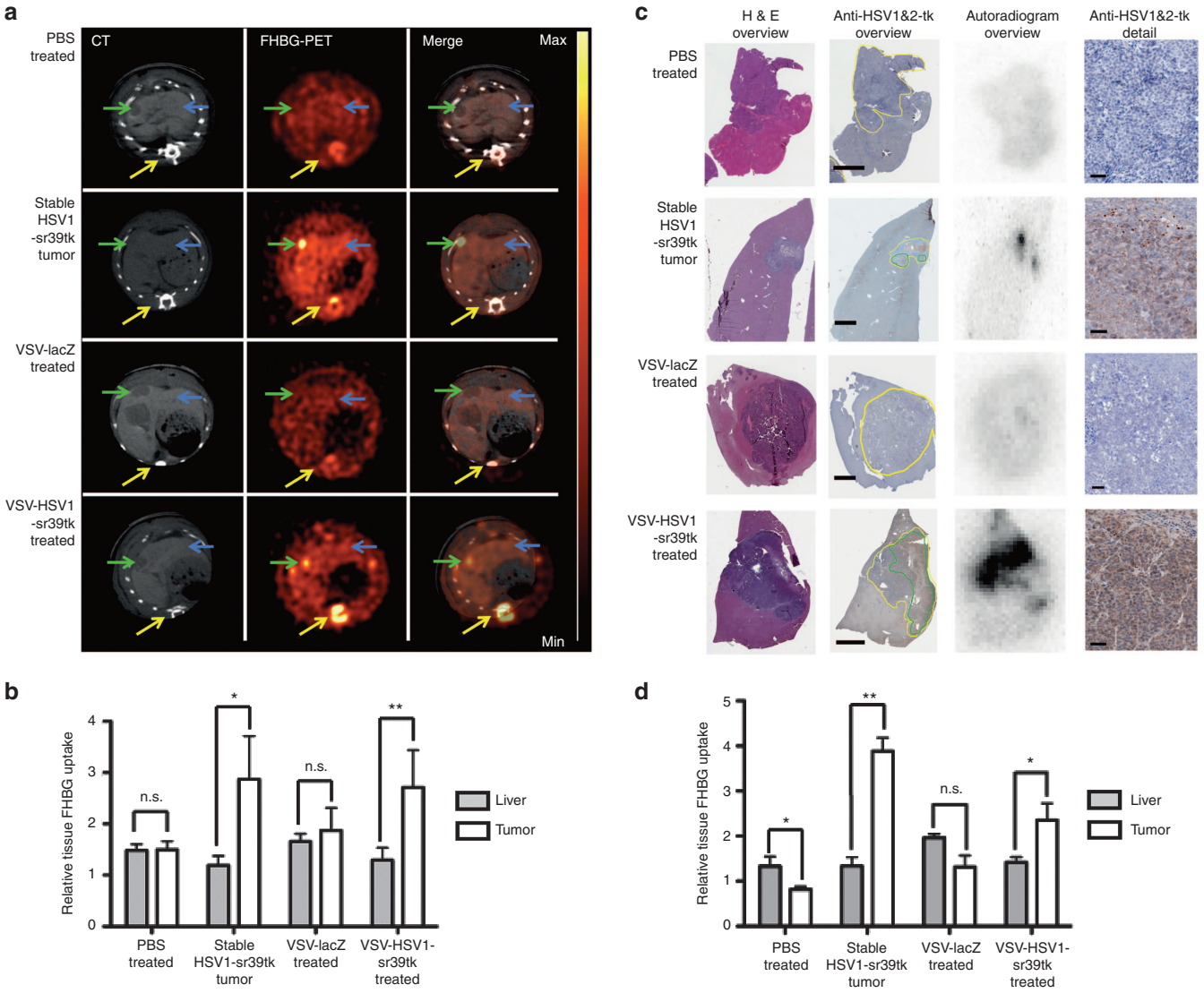

Figure 3 FHBG-PET/CT of orthotopic HCCs treated with VSV-HSV1-sr39tk. (**a**) Representative scans of rats bearing orthotopic HCCs in axial view. One representative example of every treatment group is shown in contrast-enhanced CT, PET and merged signal. Arrow heads indicate tumor (green) and liver (blue). PET intensity scale is set to 3×10^4 Bq/ml at maximum value and 0 Bq/ml at minimum value. (**b**) Semiquantitative analysis of tracer accumulation in regions of interest (ROI) from PET/CT scans. (**c**) *Ex vivo* analysis of one representative slice, containing liver tissue with orthotopic HCC lesion, of every treatment group. From left to right: HE-stained overview section, anti-HSV-1&2-tk–stained overview (tumor encircled in yellow, areas of high HSV-TK signal encircled in green) and autoradiogram of the same slice, followed by a detailed image of the anti-HSV-1&2-TK–stained tumor section. Scale bars: 1 mm (overview); 50 µm (detail). (**d**) Semiquantitative analysis of tracer accumulation in tissues of interest from *ex vivo* autoradiography analysis. All quantitative data is expressed as mean with SEM of the normalized FHBG uptake in liver and tumor, normalized to muscle, of every treatment group (groups: PBS-treated tumor $n = 4$; stable tk tumor $n = 3$; VSV-lacZ–treated tumor $n = 2$; VSV-HSV1-sr39tk–treated tumor $n = 6$). Stars indicate significance with P values lower than 0.5 (*) and 0.1 (**).

DISCUSSION

Over the last decade, substantial progress in the field of oncolytic virus development has enabled the clinical translation of OV therapy to become a reality. In light of this development, the clinical need for an accurate, sensitive, and reproducible method of noninvasively imaging the virus after application to patients has become evident. Such a system would allow clinicians to determine virus replication and biodistribution in real-time to predict the efficacy of the therapy, as well as to monitor safety, and offer the possibility of providing personalized medicine, such that the course of therapy could be altered based on imaging findings. However, noninvasive imaging of replicating viruses *in vivo* presents a unique set of challenges. Since lysis of cancerous cells occurs rapidly after infection, the time frame, in which the expression of a reporter protein can be exploited for imaging, is very limited. Due to innate differences in the replication kinetics of each vector platform, as well as the time-course of reporter protein expression versus half-life, the optimal time-point for detection of virus-mediated reporter expression needs to be determined individually for each vector and reporter system.

To date, numerous reports have described noninvasive imaging of oncolytic viruses *in vivo*[26,27,33]; however, to our knowledge, there has been no account of virus imaging in an orthotopic and immune-competent animal model of HCC. This is undoubtedly

© The American Society of Gene & Cell Therapy

due to the additional inherent technical challenges associated with these models, such as rapid immune clearance of the virus and high background in the liver due to hepatic excretion of many tracers, which consequently causes strong background accumulation and unfavorable signal-to-noise-ratios for targets located in the liver. In this study, we aimed to establish a relevant system for noninvasive imaging of oncolytic VSV for orthotopic HCC in an immune-competent host. To this end, we engineered the rVSV-HSV1-sr39tk vector and demonstrated that it allows highly sensitive imaging, with minimal background in the liver setting, for accurate monitoring of virus replication via ^{18}F-FHBG-PET and CT. All PET data in this study were validated *ex vivo* by comparison with autoradiography and immunohistochemistry of the respective tissue sections. In all cases, PET and autoradiography analyses produced nearly identical tumor:liver ratios, confirming that the PET signals did indeed originate from the tumor tissue and correlate with ^{18}F-FHBG uptake. Furthermore, by overlaying autoradiography and immunohistochemistry from the same tissue sections, we were able to determine that patterns of tracer uptake were quite similar to those of HSV-TK expression. Although signals were not completely identical, we attribute the discrepancies to differences in sensitivity of the two methods and to the fact that the thick tissue sections (about 1 mm) used for autoradiography were subsectioned to 3 µm thickness for immunohistochemistry. As a consequence, the autoradiography data represent the average of a much thicker slice of tumor. Although we were expecting homogenously high expression of HSV-TK in the stable HSV1-sr39tk–expressing tumors, we observed sparse and patchy expression patterns by immunohistochemical analysis. This observation could be partially due to low sensitivity of the antibody used, which would result in visualization of only those cells with very high HSV-TK expression. However, we believe that this observation is an accurate reflection of the loss of signal, due to the lack of drug selection and subsequent loss of gene expression *in vivo*.

Moreover, the peak in PET signal detected on day 1 after virus application with a subsequent decrease on day 3 is strongly consistent with our previous studies showing the replication kinetics of VSV in orthotopic HCC tumors, with the viral titer peaking on day 1, followed by a substantial titer reduction on day 3.[17,32]

Although we have not explicitly evaluated the efficacy of the rVSV-HSV1-sr39tk virus *in vivo* in this study, our *in vitro* data demonstrated that the recombinant vector was nearly identical to the control rVSV-lacZ vector with respect to replication kinetics and tumor cell killing. Therefore, we expect that the *in vivo* efficacy of this recombinant vector should not be significantly altered in comparison to the rVSV-lacZ vector, which we have thoroughly demonstrated in the same HCC model used in this study. With the establishment of this sensitive and robust reporter system, the potential impact in the clinical development of oncolytic virus therapy is vast. The ability to noninvasively image viral replication in real-time will allow the clinician to apply combination or prodrug therapies at the optimal time-point with respect to the viral kinetic. Furthermore, it is expected that intratumoral VSV-mediated TK signals will positively correlate to treatment outcome, and, therefore, imaging data could be potentially used as a predictive marker for therapeutic response.

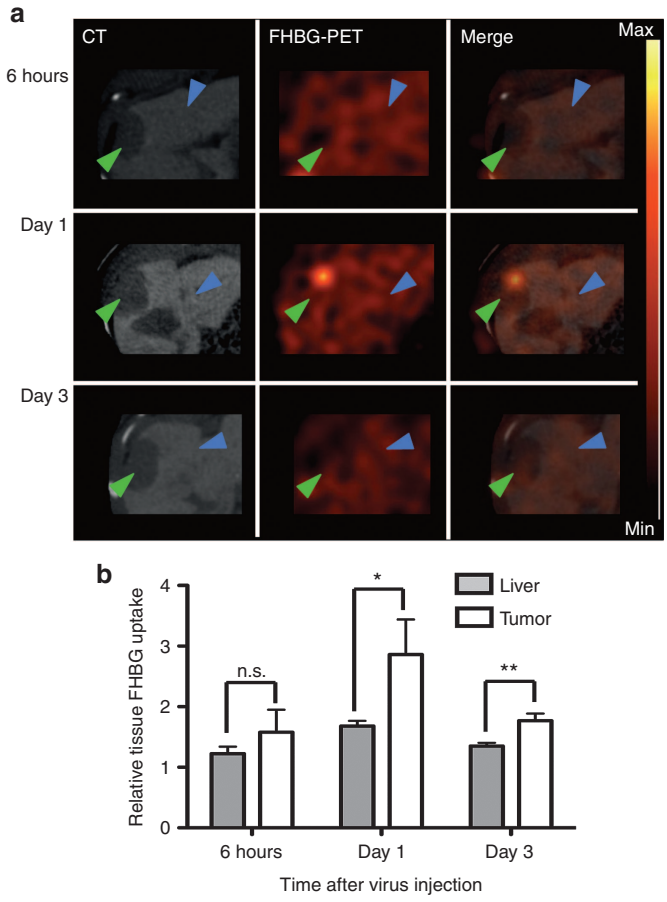

Figure 4 Detection of recombinant VSV-HSV1-sr39tk by PET is possible from day 1 after treatment. (**a**) Representative scans of rats bearing orthotopic HCCs in axial view. One representative example of every treatment group is shown in high resolution, contrast-enhanced CT, PET and merged signal. Arrows indicate tumor (green) and liver (blue). PET intensity scale refers to 3×10^4 Bq/ml at maximum value and 0 Bq/ml at minimum value. (**b**) Semiquantitative analysis of tracer accumulation in regions of interest (ROI) from PET/CT scans. Data expressed as mean and SEM of the relative FHBG uptake in liver and tumor, normalized to muscle. (Groups: 6 hours $n = 2$; day 1 $n = 4$; day 3 $n = 5$). Stars indicate significance with P values lower than 0.05 (*) and 0.01 (**).

An additional benefit of incorporation of HSV-TK into the VSV vector is the possibility of exploiting the transgene as a suicide gene and thereby enhancing the therapeutic effect of VSV upon application of the prodrug ganciclovir (GCV). The combination of HSV-TK and prodrug therapy has been shown to be effective in a clinical trial for HCC,[34] and synergistic tumor responses were reported as a result of VSV-mediated expression of the wt HSV-TK in combination with GCV in a mammary carcinoma and melanoma model.[35] However, since our study was exclusively focused on the characterization of the TK-reporting virus as an imaging vector, the additional therapeutic benefits conferred by combination therapies were beyond the experimental scope.

Of relevance, there is an abundance of evidence in the literature in support of the use of the sodium-iodide symporter (NIS) as an ideal reporter for virus imaging.[36–38] In particular, a recombinant VSV vector expressing NIS was used successfully for *in vivo* imaging in a multiple myeloma model.[33] In light of this data, our pursuit of an alternative imaging system could be

© The American Society of Gene & Cell Therapy

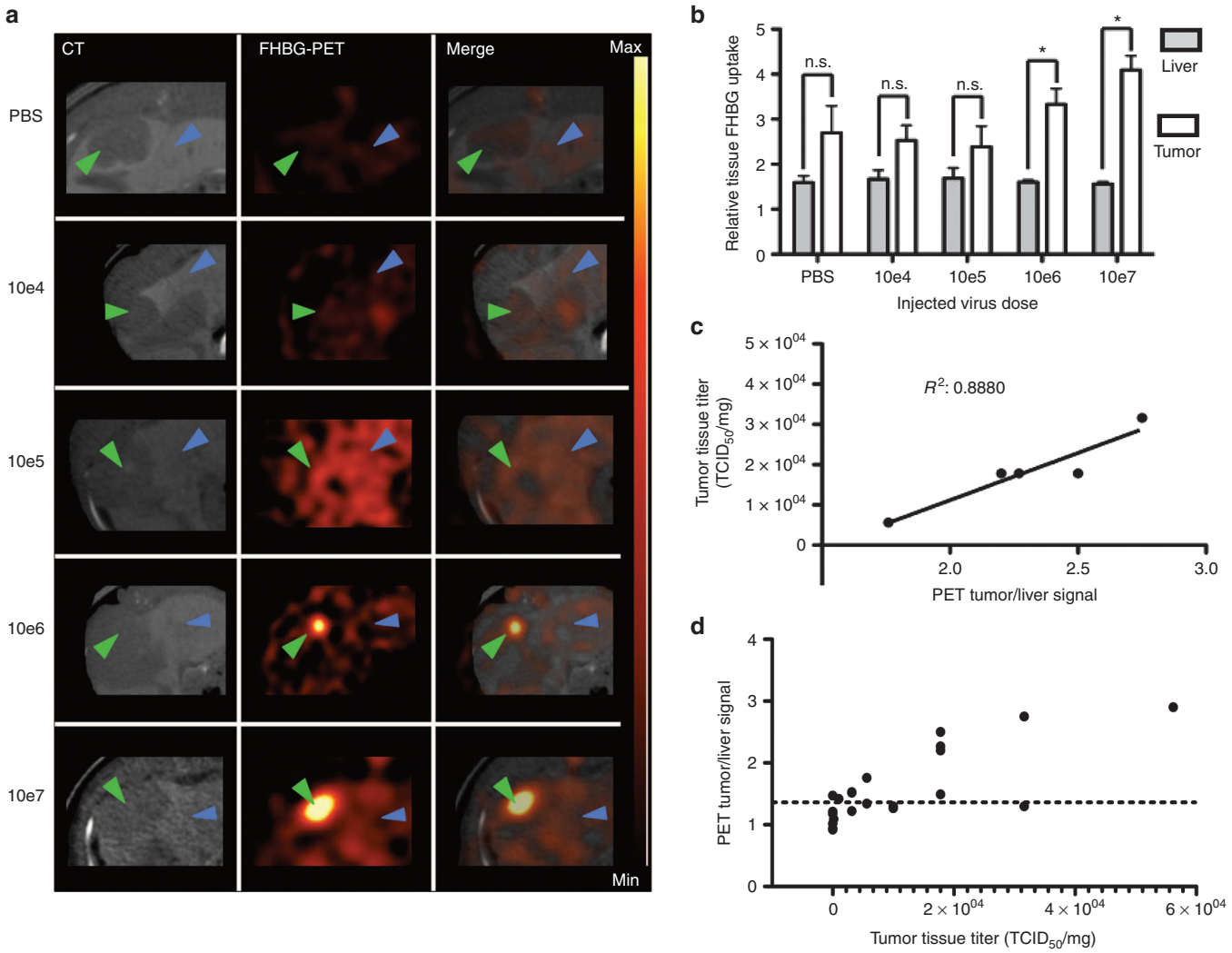

Figure 5 Recombinant VSV-HSV1-sr39tk can be detected by PET from 1×10^6 injected pfu on day 1 after application. (**a**) PET/CT scans of rats bearing orthotopic HCCs in axial view. One representative example of every treatment group is shown in high contrast-enhanced CT, PET and merged signal. Arrow heads indicate tumor (green) and liver (blue). PET intensity scale is set to 2×10^4 Bq/ml at maximum value and 5×10^3 Bq/ml at minimum value. (**b**) Semiquantitative analysis of tracer accumulation in regions of interest (ROI) from PET/CT scans. Data are expressed as mean with SEM of the relative FHBG uptake (Groups: PBS $n = 2$; 1×10^4 $n = 2$; 1×10^5 $n = 4$; 1×10^6 $n = 3$; 1×10^7 $n = 2$). Stars indicate significance with P values lower than 0.01 (*). (**c**) Correlation analysis of tumor-to-liver ROI ratios to intratumoral virus titer ($TCID_{50}$/mg). Only animals of groups, which showed significant tumor-to-liver ratios, have been analyzed for correlation. Goodness of fit was determined with $R^2 = 0.8880$. (**d**) Intratumoral virus titer (pfu/mg) versus PET tumor/liver signal of all animals. Dotted line (y = 1.33) indicates background signal (mean + SD) of PBS-treated animals ($n = 6$).

justifiably questioned. Although our initial attempts did focus on the NIS reporter, and impressive uptake of radioactive iodine in rVSV-NIS–infected cells was achieved *in vitro*, our preliminary *in vivo* characterization yielded low intratumoral signals and high background (data not shown). We concluded that rVSV-NIS was not an ideal vector for *in vivo* imaging of therapy in our orthotopic HCC model, at least partially due to the position of the liver, which results in high background signals from endogenous NIS expression in the neighboring stomach. Therefore, we aimed to identify a reporter with low or no endogenous expression, and HSV1-sr39tk proved to be an ideal candidate.

In conclusion, in this study, we have successfully established a trackable recombinant VSV, which not only maintains its efficacy for treatment of HCC, but it enables *in vivo* monitoring of virus replication. We have demonstrated HSV1-sr39tk to be an ideal reporter for VSV therapy of HCC, due to strong vector-specific signals, low background, and high correlation between viral titer and the respective PET signal. This represents a major step forward in the clinical development of VSV as an oncolytic agent for HCC, as it allows for noninvasive imaging of viral therapy to monitor safety, predict therapeutic outcome, and potentially facilitate novel combination therapies. Moreover, we envision the possibility that this tool might additionally serve as a predictor of therapy outcome, as strong virus replication, resulting in elevated PET signals, could serve as a marker for therapy responses and subsequent survival benefits. Therefore, possible correlations of the initial FHBG-PET signal after rVSV-sr39tk therapy will be a major focus of our future research. Due to establishment of our imaging system in a highly challenging preclinical model, we believe our reporter system to be highly relevant and readily translatable for

© The American Society of Gene & Cell Therapy

noninvasive tracking of oncolytic virus therapy in future clinical applications.

MATERIALS AND METHODS

Cell lines. Morris (McA-RH7777) cells (ATCC, Manassas, MA) were maintained in Dulbecco's modified Eagles medium (DMEM 30–2002; ATCC). A stable cell line was generated by transfection of an HSV1-sr39tk–expressing plasmid (a kind gift from Dr Martina Anton, TU München) with Lipofectamine 2000 (Invitrogen, life technologies, UK), followed by application of G418 for selective pressure. Resistant clones were screened by Western Blot, indirect immunofluorescence microscopy, and *in vitro* tracer uptake assays. BHK-21 cells were maintained in Glasgow Minimal Essential Medium (G-MEM BHK-21; Gibco, Life Technologies, UK) with 1% Tryptose Phosphate Broth Solution (Sigma Aldrich Company, UK). All cell culture media were supplemented with 10% fetal bovine serum and 100 U/ml penicillin/streptomycin (both purchased from Biochrome AG, Berlin, Germany). All cells were kept in a humidified atmosphere at 5% CO_2 and 37 °C.

Recombinant viruses. The HSV1-sr39tk or the lacZ gene sequences were amplified by PCR from plasmids using primers containing unique restrictions sites for *XhoI* and *NheI* for cloning into the VSV vector as an additional transcription unit at the respective cloning sites between the G- and L-protein.[39,40] After sequence confirmation, the resulting recombinant constructs were rescued as described previously[41,42] and plaque purified in BHK-21 cells.

In vitro *virus kinetics.* Morris cells were infected with either VSV-HSV1-sr39tk or VSV-lacZ at an MOI of 0.01 or 10 for 45 minutes at 37 °C and washed three times with PBS before fresh medium was added. Aliquots of supernatant were collected at several time points after infection (0, 8, 12, 24, 48, 72, and 96 hours) for determination of viral titers by 50% tissue culture infective dose ($TCID_{50}$) assay on BHK-21 cells. Cell viability was measured by MTS assay (CellTiter96 AQ_{ueous} One Solution Cell Proliferation Assay, Promega). Values are expressed as a percentage of viable cells and are normalized to respective uninfected controls at each time point.

Western blot. A 10 mg protein of whole cell lysates were analyzed by Western Blot using antibodies against HSV1-tk (Clone vL-20, Santa Cruz), VSV-G (anti-VSV-G epitope tag antibody 600-401-386; Rockland antibodies and assays; Gilbertsville) and β-actin (Clone AC-40, Sigma-Aldrich), and detected by Amersham ECL (ECL Prime Western Blotting Detection Reagent, GE Healthcare, UK) as recommended by the manufacturer.

Indirect immunofluorescence microscopy. Cells plated in chamber slides were infected at an MOI of 1 for 8 hrs. Immunofluorescence was performed using antibodies against VSV-G (see above) and HSV-tk (Clone 2C5.2; Bioworld Consulting Laboratories). Counterstaining was done by Hoechst (Hoechst 3342, Thermo Fisher Scientific) before mounting with Roti-Mount FluorCare (Carl Roth, Germany).

^{18}F-FHBG* in vitro *uptake. Cells were plated in 12-well plates and treated with PBS or infected at an MOI of 0.1. After 16 hours, 1 MBq of ^{18}F-FHBG was added to each well, and cells were incubated at 37 °C for 45 minutes before washing twice with ice-cold PBS and lysing with 1 N NaOH. ^{18}F-FHBG uptake was measured in a γ-counter, and uptake values were normalized to the cell number.

Animal models. All animal protocols were approved by the regional governmental commission for animal protection (Regierung von Oberbayern, Munich, Germany). Male 6- to 10-week-old Buffalo rats were implanted with syngeneic Morris HCC cells. Orthotopic tumors were established as previously described,[17] and treated by intratumoral injection of 100 µl of virus or PBS on day 10, when the tumors had reached a size of 0.5–1 cm in diameter. For the subcutaneous HCC model, 10^6 cells were injected in the left (wt) or right (stable HSV1-sr39tk) shoulder. After 14 days, tumors reached a size of ~1 cm in diameter.

PET/CT imaging. Animals were imaged using a state-of-the-art small-animal PET/CT scanner (Inveon, Siemens Medical Solutions). ^{18}F-FHBG was prepared as previously described.[43] Image acquisition was performed 2 hours after intravenous injection of 40 MBq of ^{18}F-FHBG for 15 minutes under isoflurane anesthesia. PET data were reconstructed using a OSEM3D algorithm, normalized and corrected for randoms, dead time and decay. CT contrast agent ExiTron nano12000 (Miltenyi Biotec GmbH, Germany)[44] was applied 1 day before imaging (1 ml/kg i.v.). A background CT scan was performed for anatomical localization.

Image analysis. Image analysis was performed on the INVEON Research Workplace (Siemens, Knoxville, TN). CT and PET images were coregistered, and three-dimensional regions of interest (ROIs) were drawn (liver, whole tumor, spinal muscle) based on the CT image. For measuring the tumor uptake, a 50% threshold was applied (mean of the hottest 50% within the entire tumor ROI, as defined by CT image). Semiquantitative analysis was performed with mean activities from the ROIs expressed as Bq/ml and normalized to the muscle uptake.

Autoradiography. *Ex vivo* autoradiography analysis of tumor, liver, and muscle was performed postimaging. Three slices of each tissue were fixed with 4% paraformaldehyde and exposed overnight to an image plate (biostep, Jahnsdorf, Germany), before scanning by an image plate scanner (CR 35 BIO, Dürr Medical, Raytest Isotopenmeßgeräte GmbH, Germany) at an internal sensitive resolution of 50 µm. Analysis was performed with AIDA Image Analyser Software (Raytest Isotopenmeßgeräte, Germany) by carefully aligning the autoradiography signal to the histology of each slice. All tissue uptake values were normalized to muscle values and are, therefore, semiquantitative.

Histology and immunohistochemistry. After autoradiography, tissues were embedded in paraffin, and serial sections were stained with hematoxylin-eosin (HE). Immunohistochemistry against HSV-tk (Clone 2C5.2; Bioworld Consulting Laboratories) was performed using a Dako Autostainer (Dako) after standard HIER procedure. The slides were analyzed by two blinded pathologists, and the areas of HSV-tk expression were marked.

Statistical analysis. Excel (Microsoft Office) and Prism (GraphPad Software) were used for data handling, statistical analysis and graphic layout. Significance was tested by unpaired *t*-test, and one-tailed *P* values have been analyzed.

ACKNOWLEDGMENTS

We thank Sybille Reder, Markus Mittelhäuser, and Marco Lehmann for assistance on performing PET imaging, Michael Herz for tracer preparation and Martina Anton for help with *in vitro* tracer uptake assays. The research leading to these results has received funding from the Deutsche Forschungsgemeinschaft (DFG) under Grant Agreement No. SFB 824 subprojects C7, Z1, Z2, and Z3. The authors declare no conflict of interest.

REFERENCES

1. Altekruse, SF, McGlynn, KA and Reichman, ME (2009). Hepatocellular carcinoma incidence, mortality, and survival trends in the United States from 1975 to 2005. *J Clin Oncol* **27**: 1485–1491.
2. Kim, WR, Gores, GJ, Benson, JT, Therneau, TM and Melton, LJ 3rd (2005). Mortality and hospital utilization for hepatocellular carcinoma in the United States. *Gastroenterology* **129**: 486–493.
3. Yao, FY, Bass, NM, Nikolai, B, Davern, TJ, Kerlan, R, Wu, V *et al.* (2002). Liver transplantation for hepatocellular carcinoma: analysis of survival according to the intention-to-treat principle and dropout from the waiting list. *Liver Transpl* **8**: 873–883.
4. Yeung, YP, Lo, CM, Liu, CL, Wong, BC, Fan, ST and Wong, J (2005). Natural history of untreated nonsurgical hepatocellular carcinoma. *Am J Gastroenterol* **100**: 1995–2004.
5. Yang, JD and Roberts, LR (2010). Hepatocellular carcinoma: A global view. *Nat Rev Gastroenterol Hepatol* **7**: 448–458.

© The American Society of Gene & Cell Therapy

6. Capocaccia, R, Sant, M, Berrino, F, Simonetti, A, Santi, V and Trevisani, F; EUROCARE Working Group (2007). Hepatocellular carcinoma: trends of incidence and survival in Europe and the United States at the end of the 20th century. *Am J Gastroenterol* **102**: 1661–70; quiz 1660, 1671.
7. Russell, SJ and Peng, KW (2007). Viruses as anticancer drugs. *Trends Pharmacol Sci* **28**: 326–333.
8. Kelly, E and Russell, SJ (2007). History of oncolytic viruses: genesis to genetic engineering. *Mol Ther* **15**: 651–659.
9. Russell, SJ, Peng, KW and Bell, JC (2012). Oncolytic virotherapy. *Nat Biotechnol* **30**: 658–670.
10. Cattaneo, R, Miest, T, Shashkova, EV and Barry, MA (2008). Reprogrammed viruses as cancer therapeutics: targeted, armed and shielded. *Nat Rev Microbiol* **6**: 529–540.
11. Dorer, DE and Nettelbeck, DM (2009). Targeting cancer by transcriptional control in cancer gene therapy and viral oncolysis. *Adv Drug Deliv Rev* **61**: 554–571.
12. Heo, J, Reid, T, Ruo, L, Breitbach, CJ, Rose, S, Bloomston, M *et al.* (2013). Randomized dose-finding clinical trial of oncolytic immunotherapeutic vaccinia JX-594 in liver cancer. *Nat Med* **19**: 329–336.
13. Patel, MR and Kratzke, RA (2013). Oncolytic virus therapy for cancer: the first wave of translational clinical trials. *Transl Res* **161**: 355–364.
14. Hastie, E and Grdzelishvili, VZ (2012). Vesicular stomatitis virus as a flexible platform for oncolytic virotherapy against cancer. *J Gen Virol* **93**(Pt 12): 2529–2545.
15. Altomonte, J, Braren, R, Schulz, S, Marozin, S, Rummeny, EJ, Schmid, RM *et al.* (2008). Synergistic antitumor effects of transarterial viroembolization for multifocal hepatocellular carcinoma in rats. *Hepatology* **48**: 1864–1873.
16. Altomonte, J, Wu, L, Meseck, M, Chen, L, Ebert, O, Garcia-Sastre, A *et al.* (2009). Enhanced oncolytic potency of vesicular stomatitis virus through vector-mediated inhibition of NK and NKT cells. *Cancer Gene Ther* **16**: 266–278.
17. Ebert, O, Shinozaki, K, Huang, TG, Savontaus, MJ, García-Sastre, A and Woo, SL (2003). Oncolytic vesicular stomatitis virus for treatment of orthotopic hepatocellular carcinoma in immune-competent rats. *Cancer Res* **63**: 3605–3611.
18. Altomonte, J, Marozin, S, De Toni, EN, Rizzani, A, Esposito, I, Steiger, K *et al.* (2013). Antifibrotic properties of transarterial oncolytic VSV therapy for hepatocellular carcinoma in rats with thioacetamide-induced liver fibrosis. *Mol Ther* **21**: 2032–2042.
19. Jenks, N, Myers, R, Greiner, SM, Thompson, J, Mader, EK, Greenslade, A *et al.* (2010). Safety studies on intrahepatic or intratumoral injection of oncolytic vesicular stomatitis virus expressing interferon-beta in rodents and nonhuman primates. *Hum Gene Ther* **21**: 451–462.
20. Räty, JK, Liimatainen, T, Unelma Kaikkonen, M, Gröhn, O, Airenne, KJ, Jumani Airenne, K *et al.* (2007). Non-invasive Imaging in Gene Therapy. *Mol Ther* **15**: 1579–1586.
21. Tjuvajev, JG, Doubrovin, M, Akhurst, T, Cai, S, Balatoni, J, Alauddin, MM *et al.* (2002). Comparison of radiolabeled nucleoside probes (FIAU, FHBG, and FHPG) for PET imaging of HSV1-tk gene expression. *J Nucl Med* **43**: 1072–1083.
22. Chan, PC, Wu, CY, Chang, WY, Chang, WT, Alauddin, M, Liu, RS *et al.* (2011). Evaluation of F-18-labeled 5-iodocytidine (18F-FIAC) as a new potential positron emission tomography probe for herpes simplex virus type 1 thymidine kinase imaging. *Nucl Med Biol* **38**: 987–995.
23. Tian, H, Lu, X, Guo, H, Corn, D, Molter, J, Wang, B *et al.* (2012). Radio-deoxynucleoside Analogs used for Imaging tk Expression in a Transgenic Mouse Model of Induced Hepatocellular Carcinoma. *Theranostics* **2**: 597–606.
24. Lu, X, Guo, H, Molter, J, Miao, H, Gerber, L, Hu, Y *et al.* (2011). Alpha-fetoprotein-thymidine kinase-luciferase knockin mice: a novel model for dual modality longitudinal imaging of tumorigenesis in liver. *J Hepatol* **55**: 96–102.
25. Gambhir, SS, Bauer, E, Black, ME, Liang, Q, Kokoris, MS, Barrio, JR *et al.* (2000). A mutant herpes simplex virus type 1 thymidine kinase reporter gene shows improved sensitivity for imaging reporter gene expression with positron emission tomography. *Proc Natl Acad Sci USA* **97**: 2785–2790.
26. Peñuelas, I, Mazzolini, G, Boán, JF, Sangro, B, Martí-Climent, J, Ruiz, M *et al.* (2005). Positron emission tomography imaging of adenoviral-mediated transgene expression in liver cancer patients. *Gastroenterology* **128**: 1787–1795.
27. Pañeda, A, Collantes, M, Beattie, SG, Otano, I, Snapper, J, Timmermans, E *et al.* (2011). Adeno-associated virus liver transduction efficiency measured by *in vivo* [18F] FHBG positron emission tomography imaging in rodents and nonhuman primates. *Hum Gene Ther* **22**: 999–1009.
28. Alauddin, MM, Shahinian, A, Gordon, EM and Conti, PS (2004). Direct comparison of radiolabeled probes FMAU, FHBG, and FHPG as PET imaging agents for HSV1-tk expression in a human breast cancer model. *Mol Imaging* **3**: 76–84.
29. Buursma, AR, Rutgers, V, Hospers, GA, Mulder, NH, Vaalburg, W and de Vries, EF (2006). 18F-FEAU as a radiotracer for herpes simplex virus thymidine kinase gene expression: in-vitro comparison with other PET tracers. *Nucl Med Commun* **27**: 25–30.
30. Yaghoubi, S, Barrio, JR, Dahlbom, M, Iyer, M, Namavari, M, Satyamurthy, N *et al.* (2001). Human pharmacokinetic and dosimetry studies of [(18)F]FHBG: a reporter probe for imaging herpes simplex virus type-1 thymidine kinase reporter gene expression. *J Nucl Med* **42**: 1225–1234.
31. Yaghoubi, SS, Couto, MA, Chen, CC, Polavaram, L, Cui, G, Sen, L *et al.* (2006). Preclinical safety evaluation of 18F-FHBG: a PET reporter probe for imaging herpes simplex virus type 1 thymidine kinase (HSV1-tk) or mutant HSV1-sr39tk's expression. *J Nucl Med* **47**: 706–715.
32. Shinozaki, K, Ebert, O, Kournioti, C, Tai, YS and Woo, SL (2004). Oncolysis of multifocal hepatocellular carcinoma in the rat liver by hepatic artery infusion of vesicular stomatitis virus. *Mol Ther* **9**: 368–376.
33. Goel, A, Carlson, SK, Classic, KL, Greiner, S, Naik, S, Power, AT *et al.* (2007). Radioiodide imaging and radiovirotherapy of multiple myeloma using VSV(Delta51)-NIS, an attenuated vesicular stomatitis virus encoding the sodium iodide symporter gene. *Blood* **110**: 2342–2350.
34. Sangro, B, Mazzolini, G, Ruiz, M, Ruiz, J, Quiroga, J, Herrero, I *et al.* (2010). A phase I clinical trial of thymidine kinase-based gene therapy in advanced hepatocellular carcinoma. *Cancer Gene Ther* **17**: 837–843.
35. Fernandez, M, Porosnicu, M, Markovic, D and Barber, GN (2002). Genetically engineered vesicular stomatitis virus in gene therapy: application for treatment of malignant disease. *J Virol* **76**: 895–904.
36. Haddad, D, Zanzonico, PB, Carlin, S, Chen, CH, Chen, NG, Zhang, Q *et al.* (2012). A vaccinia virus encoding the human sodium iodide symporter facilitates long-term image monitoring of virotherapy and targeted radiotherapy of pancreatic cancer. *J Nucl Med* **53**: 1933–1942.
37. Grünwald, GK, Vetter, A, Klutz, K, Willhauck, MJ, Schwenk, N, Senekowitsch-Schmidtke, R *et al.* (2013). Systemic image-guided liver cancer radiovirotherapy using dendrimer-coated adenovirus encoding the sodium iodide symporter as theranostic gene. *J Nucl Med* **54**: 1450–1457.
38. Reddi, HV, Madde, P, McDonough, SJ, Trujillo, MA, Morris, JC 3rd, Myers, RM *et al.* (2012). Preclinical efficacy of the oncolytic measles virus expressing the sodium iodide symporter in iodine non-avid anaplastic thyroid cancer: a novel therapeutic agent allowing noninvasive imaging and radioiodine therapy. *Cancer Gene Ther* **19**: 659–665.
39. Lawson, ND, Stillman, EA, Whitt, MA and Rose, JK (1995). Recombinant vesicular stomatitis viruses from DNA. *Proc Natl Acad Sci USA* **92**: 4477–4481.
40. Whelan, SP, Ball, LA, Barr, JN and Wertz, GT (1995). Efficient recovery of infectious vesicular stomatitis virus entirely from cDNA clones. *Proc Natl Acad Sci USA* **92**: 8388–8392.
41. Schnell, MJ, Buonocore, L, Kretzschmar, E, Johnson, E and Rose, JK (1996). Foreign glycoproteins expressed from recombinant vesicular stomatitis viruses are incorporated efficiently into virus particles. *Proc Natl Acad Sci USA* **93**: 11359–11365.
42. Schnell, MJ, Buonocore, L, Whitt, MA and Rose, JK (1996). The minimal conserved transcription stop-start signal promotes stable expression of a foreign gene in vesicular stomatitis virus. *J Virol* **70**: 2318–2323.
43. Alauddin, MM and Conti, PS (1998). Synthesis and preliminary evaluation of 9-(4-[18F]-fluoro-3-hydroxymethylbutyl)guanine ([18F]FHBG): a new potential imaging agent for viral infection and gene therapy using PET. *Nucl Med Biol* **25**: 175–180.
44. Boll, H, Nittka, S, Doyon, F, Neumaier, M, Marx, A, Kramer, M *et al.* (2011). Micro-CT based experimental liver imaging using a nanoparticulate contrast agent: a longitudinal study in mice. *PLoS ONE* **6**: e25692.